BIT Numerical Mathematics (2024) 64:36
https://doi.org/10.1007/s10543-024-01037-6

BIT

Pressure-robust approximation of the incompressible Navier–Stokes equations in a rotating frame of reference

Medine Demir[1] · **Volker John**[1,2]

Received: 23 November 2023 / Accepted: 28 August 2024

Abstract
A pressure-robust space discretization of the incompressible Navier–Stokes equations in a rotating frame of reference is considered. The discretization employs divergence-free, H^1-conforming mixed finite element methods like Scott–Vogelius pairs. An error estimate for the velocity is derived that tracks the dependency of the error bound on the coefficients of the problem, in particular on the angular velocity. Numerical examples support the theoretical results.

Keywords Navier–Stokes equations in rotating frame of reference · Coriolis force · Scott–Vogelius pairs of finite element spaces · Pressure-robust error estimate

Mathematics Subject Classification 65M60

1 Introduction

Most of the computational fluid dynamics (CFD) applications both in physics and engineering deal with flows observed from a fixed (inertial or absolute) frame of reference. Such flows are governed by the well-known Navier–Stokes equations. In a fixed reference frame, Newton's first and second laws of motion can be applied directly in inertial frame. However, the Earth is rotating and there are important fluid flows in meteorology and oceanography, especially in the large-scale flows considered in ocean and atmosphere, dominated by the rotating effects of the Earth. It might be therefore more convenient to describe the flow relative to the Earth's surface rather than an inertial frame. In addition to this, there is also a broad class of physical and industrial applications with rotating systems with fluids [3, 10]. In the literature, there are several

Communicated by Martin Kronbichler.

✉ Medine Demir
demir@wias-berlin.de

[1] Weierstrass Institute for Applied Analysis and Stochastic, 10117 Berlin, Germany

[2] Department of Mathematics and Computer Science, Freie Universität of Berlin, 14195 Berlin, Germany

Published online: 18 September 2024

popular numerical techniques to handle problems with rotating systems (or more generally with time-dependent domains), e.g., the Arbitrary Lagrangian–Eulerian method (ALE) [17, 18], which works with fluid quantities defined in a stationary inertial reference frame. In the ALE method, mesh lines are constantly moved to account for the movement of the domain.

Mapping the inertial frame to the time-dependent domain introduces an additional transport term that is induced by the grid velocity. For the special case of a rotating system, the method of performing computations in a moving (non-inertial) reference frame has been proposed as an alternative way for flow simulations. In this method, the flow problem is transformed from the inertial frame to the rotating frame. The fluid observed in a rotating frame of reference has accelerating velocity. Therefore, the formulation of Newton's second law of motion in a rotating frame of reference has to take into account the effects of coordinate acceleration by introducing two forces in the statement of Newton's second law; namely the centripetal and the Coriolis forces. An attractive feature of using a rotating frame of reference is that the computational mesh is fixed and rotating boundaries do not slip relative to the rotating frame, since they are moving at the same speed as the reference frame. Additionally, it is suitable for both steady-state and transient simulations of these problems.

This paper considers discretizations of the incompressible Navier–Stokes equations in a rotating frame of reference, which are given by

$$\begin{aligned} \rho\partial_t \boldsymbol{u} - \mu\Delta\boldsymbol{u} + \rho(\boldsymbol{u}\cdot\nabla)\boldsymbol{u} + 2\rho\boldsymbol{\omega}\times\boldsymbol{u} + \nabla p &= \boldsymbol{f} - \rho\boldsymbol{\omega}\times(\boldsymbol{\omega}\times\boldsymbol{r}) && \text{in } (0,T]\times\Omega, \\ \nabla\cdot\boldsymbol{u} &= 0 && \text{in } (0,T]\times\Omega. \end{aligned} \tag{1.1}$$

Here, $\boldsymbol{u}$ [m/s] and p [Pa] denote the unknown velocity field and the unknown pressure of the flow, relative to the rotating frame of reference. The physical coefficients ρ [kg/m^3] > 0, μ [kg/ms] > 0 and $\boldsymbol{\omega}$ [1/s] $\neq \mathbf{0}$ denote the density of the fluid, the dynamic viscosity of the fluid, and the angular velocity vector of the rotating frame of reference, respectively. These quantities are given. The density and dynamic viscosity are assumed to be positive constants and the kinematic viscosity is defined by $\nu = \mu/\rho$ [m^2/s]. The body force per volume acting on the fluid is denoted by $\boldsymbol{f}$ [N/m^3]. It is assumed that the origin of the coordinate system meets the axis of rotation. The position vector is denoted by $\boldsymbol{r}$ [m]. Then, $2\rho\boldsymbol{\omega}\times\boldsymbol{u}$ and $\rho\boldsymbol{\omega}\times(\boldsymbol{\omega}\times\boldsymbol{r})$ model the Coriolis and the centripetal forces, respectively. The problem is posed in a bounded Lipschitz continuous domain $\Omega \subset \mathbb{R}^d$, $d \in \{2, 3\}$, and in a finite time interval $(0, T]$. It will be considered with homogeneous Dirichlet boundary conditions

$$\boldsymbol{u}(t,\boldsymbol{x}) = \mathbf{0} \quad \text{in } [0,T]\times\partial\Omega,$$

where $\partial\Omega$ is the boundary of Ω. Finally, an initial condition

$$\boldsymbol{u}(0,\boldsymbol{x}) = \boldsymbol{u}_0(\boldsymbol{x}) \quad \text{in } \Omega$$

has to be prescribed.

The Coriolis and the centripetal forces, resulting from the rotation of the Earth, play a crucial role in understanding the behavior of rotating flows. The Coriolis force acts on all moving bodies in a rotating frame of reference and can be thought in terms of angular momentum conservation. Since it is perpendicular to the fluid velocity, it has no effect on fluid parcels (small volumes of fluid) and only leads to a deflection of the fluid to the right (in the Northern hemisphere). The centripetal force is perpendicular to the axis of rotation and is directed radially towards the center of rotation. Approximating the solution of (1.1) accurately poses several difficulties. On the one hand, one has to deal with the usual challenges in approximating problems of Navier–Stokes type which are nonlinearity, which require to satisfy or circumvent the well-known discrete inf-sup condition, and which comprise dominant convection in the turbulent regime, see [20]. In addition, for (1.1) one has to properly handle the extra forces.

In recent years, the Navier–Stokes equations in a rotating frame have been investigated in a number of papers to contribute to the analysis and the accurate and efficient numerical simulation. For example, Refs. [14, 16, 19, 22] studied the global well-posedness of (1.1) with uniformly small initial data $\boldsymbol{u}_0$. A discrete projection method was analyzed both theoretically and numerically for problem (1.1) in [25, 29]. An error analysis of the incremental pressure-correction projection scheme is presented in [30]. The analysis of an operator splitting method for the numerical solution of (1.1) can be found in [28]. All these paper study the splitting error and it is shown that the results from the standard Navier–Stokes equations carry over to (1.1). The stability of an implicit-explicit (IMEX) method for mixed finite element discretizations of the Navier–Stokes equations in a rotating frame of reference is studied in [2].

It should be noted that the pressure gradient, which is like a Lagrange multiplier to enforce the incompressibility constraint $\nabla \cdot \boldsymbol{u} = 0$, plays a special role in the incompressible Navier–Stokes equations. The pressure gradient is incorporated in the momentum equation to balance any occurring, unbalanced gradient-type force in the momentum balance. In the special situation that the angular velocity is a constant vector with respect to space, the centripetal force can be written as a gradient

$$\rho\boldsymbol{\omega} \times (\boldsymbol{\omega} \times \boldsymbol{r}) = -\nabla\phi_c \quad \text{with} \quad \phi_c = \frac{\rho}{2}\|\boldsymbol{\omega} \times \boldsymbol{r}\|_2^2, \tag{1.2}$$

where $\|\cdot\|_2$ denotes the Euclidean norm of a vector. Thus, a strong gradient force might be present on the right-hand side of (1.1), depending on the angular velocity. And even if $\boldsymbol{\omega}$ is not constant, the gradient part of the Helmholtz decomposition of the centripetal force might be large. Since gradient-type forces on the right-hand side of (1.1) have to be balanced by the pressure, the centripetal force might induce large pressure values and pressure gradients, compare also Sect. 4.2 below.

It is well known that in most of the classical inf-sup stable pairs of finite element spaces for approximating the incompressible Navier–Stokes equations, like the H^1-conforming Taylor–Hood pairs, the conservation of mass is only discretely enforced and so the discrete solutions are not weakly divergence-free, i.e., the $L^2(\Omega)$ norm of the divergence does not vanish. Numerical analysis shows that the error of the divergence behaves similar to the error of the velocity gradient, thus potentially resulting in poor mass conservation, in particular when the viscosity ν is small, e.g., see [21].

Numerical analysis for the standard incompressible Navier–Stokes equations reveals also that classical methods, like Taylor–Hood pairs, introduce a pressure-dependent contribution in velocity error bounds that is proportional to some inverse power of the viscosity, e.g., see [21, 24]. Hence, these methods are optimally convergent but small velocity errors might not be achieved for large pressures and small viscosity coefficients. Such methods are called to be not pressure-robust. Several approaches have been proposed for improving the pressure robustness of such pairs of finite element spaces, like grad-div stabilization [5, 24] or using appropriate reconstructions of functions [23]. The drawback of large pressure contributions in velocity error bounds can be avoided by using pairs of finite element spaces that lead to weakly divergence-free discrete velocity solutions, like Scott–Vogelius pairs. Such pairs give mass conservation, they are inf-sup stable on special grids [27, 31], and satisfy optimal approximation properties, where the velocity bounds are independent of the pressure.

In the present paper, it will be shown that these favorable properties carry over to the discretization of (1.1) with Scott–Vogelius pairs. Compared with the standard Navier–Stokes equations, two additional terms appear in (1.1) and, as already mentioned, large pressures might be induced by large centripetal forces. To the best of the authors' knowledge, until now, no pressure-robust mixed method has been proposed and analyzed for these equations. It will be shown that the method is stable and satisfies an energy equality. A velocity error estimate will be derived that is pressure-robust. The error bound does not depend explicitly on negative powers of the viscosity, but there is a dependency on the angular velocity. As usual, the numerical analysis assumes sufficient regularity of the solution of (1.1). Numerical studies will support the analytic results.

The remainder of the paper is organized as follows. Section 2 provides some notations and mathematical preliminaries needed for the numerical analysis. In addition, the discretization with the Scott–Vogelius pair of finite element spaces is introduced. Section 3 is devoted to the numerical analysis of the method. Numerical studies for verifying the analytic results are presented in Sect. 4. Finally, Sect. 5 provides a summary and an outlook.

2 Weak formulation and finite element discretization

Standard notations for Sobolev spaces and their norms will be used. In particular, the inner product in $L^2(\Omega)^d$, $d \geq 1$, is denoted by $(\cdot, \cdot)$ and the induced norm by $\| \cdot \|_0$. Sobolev spaces on Ω are denoted by $H^r(\Omega)$, $r \in \mathbb{R}$, $r > 0$, with the corresponding norm $\| \cdot \|_r$. The space $H_0^1(\Omega)$ contains all functions from $H^1(\Omega)$ with vanishing trace on $\partial\Omega$. Spaces for vector-valued functions are indicated with bold face symbols. Function spaces in spatio-temporal domains are denoted as usual with the time interval and the spatial function as arguments.

The space of weakly divergence-free functions is defined by

$$\boldsymbol{H}_{\mathrm{div}}(\Omega) = \Big\{ \boldsymbol{v} \in \boldsymbol{L}^2(\Omega) \;\; \nabla \cdot \boldsymbol{v} \in L^2(\Omega), \;\; -(\boldsymbol{v}, \nabla \psi) = 0 \; \forall \, \psi \in H^1(\Omega) \\ \text{and } \boldsymbol{v} \cdot \boldsymbol{n} = 0 \big\},$$

with $\boldsymbol{n}$ being the unit outer normal at $\partial\Omega$. Note that $\|\nabla\cdot\boldsymbol{v}\|_0 = 0$ for all $\boldsymbol{v}\in\boldsymbol{H}_{\mathrm{div}}(\Omega)$. If a weakly divergence-free function is even from $\boldsymbol{H}_0^1(\Omega)$, then the corresponding subspace is denoted by

$$\boldsymbol{V}_{\mathrm{div}} = \left\{\boldsymbol{v}\in\boldsymbol{H}_0^1(\Omega)\ \ \|\nabla\cdot\boldsymbol{v}\|_0 = 0\right\}.$$

Then, a weak formulation of (1.1) with time-independent velocity test functions $\boldsymbol{v}\in\boldsymbol{V}_{\mathrm{div}}$ for computing the velocity $\boldsymbol{u}\in L^2(0,T;\boldsymbol{V}_{\mathrm{div}})\cap L^\infty(0,T;\boldsymbol{H}_{\mathrm{div}}(\Omega))$ is given by

$$\begin{aligned}\rho(\partial_t\boldsymbol{u},\boldsymbol{v}) + \mu(\nabla\boldsymbol{u},\nabla\boldsymbol{v}) + \rho((\boldsymbol{u}\cdot\nabla)\boldsymbol{u},\boldsymbol{v}) + 2(\boldsymbol{\omega}\times\boldsymbol{u},\boldsymbol{v})\\ = \langle\boldsymbol{f},\boldsymbol{v}\rangle_{\boldsymbol{H}^{-1},\boldsymbol{H}_0^1} - \rho(\boldsymbol{\omega}\times(\boldsymbol{\omega}\times\boldsymbol{r}),\boldsymbol{v})\end{aligned} \tag{2.1}$$

for all $\boldsymbol{v}\in\boldsymbol{V}_{\mathrm{div}}$, where $\boldsymbol{\omega}\in L^\infty(0,T;L^\infty(\Omega))$ and $\boldsymbol{f}\in L^2\left(0,T;\boldsymbol{H}^{-1}(\Omega)\right)$ are assumed and the symbol of the first term on the right-hand side denotes the dual pairing of the spaces indicated by the subscript. The pressure does not occur in this weak formulation because it is a gradient that is tested with a weakly divergence-free function. For the initial velocity field it is assumed that $\boldsymbol{u}_0(\boldsymbol{x})\in\boldsymbol{H}_{\mathrm{div}}(\Omega)$.

Let $\{\mathcal{T}_h\}$, $h>0$, be a family of admissible and shape-regular triangulations of Ω. For the discretization in space, the Scott–Vogelius pair of finite element spaces $(\boldsymbol{V}_h, Q_h) = (\boldsymbol{P}_r, P_{r-1}^{\mathrm{disc}})$, proposed in [27], for approximating velocity and pressure will be considered, i.e., the velocity is approximated by a continuous finite element function that is a piecewise polynomial of degree r and the pressure by a discontinuous finite element function that is a piecewise polynomial of degree $r-1$. In particular it holds $\boldsymbol{V}_h\subset\boldsymbol{H}_0^1(\Omega)$. An attractive property of the Scott–Vogelius element is that the discrete divergence-free constraint

$$(\nabla\cdot\boldsymbol{u}_h, q_h) = 0\quad\forall\, q_h\in Q_h,$$

implies even that $\boldsymbol{u}_h$ is weakly divergence-free, i.e., it holds $\|\nabla\cdot\boldsymbol{u}_h\|_0 = 0$, which follows by the special choice of $q_h = \nabla\cdot\boldsymbol{u}_h$, which is possible due to $\nabla\cdot\boldsymbol{V}_h\subset Q_h$. Consequently, the discretely divergence-free subspace of $\boldsymbol{V}_h$ can be characterized as follows

$$\begin{aligned}\boldsymbol{V}_{h,\mathrm{div}} &= \{\boldsymbol{v}_h\in\boldsymbol{V}_h\ \ (\nabla\cdot\boldsymbol{v}_h, q_h) = 0,\ \forall\, q_h\in Q_h\}\\ &= \{\boldsymbol{v}_h\in\boldsymbol{V}_h\ \ \|\nabla\cdot\boldsymbol{v}_h\|_0 = 0\}.\end{aligned}$$

Thus, the elements of $\boldsymbol{V}_{h,\mathrm{div}}$ are weakly divergence-free, i.e., $\boldsymbol{V}_{h,\mathrm{div}}\subset\boldsymbol{H}_{\mathrm{div}}(\Omega)$, and mass conservation is achieved for the discrete problem.

Scott–Vogelius pairs are known to fulfil the discrete inf-sup condition

$$\inf_{0\neq q_h\in Q_h}\sup_{\boldsymbol{0}\neq\boldsymbol{v}_h\in\boldsymbol{V}_h}\frac{(\nabla\cdot\boldsymbol{v}_h,\ q_h)}{\|\nabla\boldsymbol{v}_h\|_0\|q_h\|_0} = \beta_h > 0, \tag{2.2}$$

independently of the mesh width under certain restrictions on the mesh and polynomial degree, e.g.,

- If $d = 2$, $r \geq 4$, and the mesh has no singular vertices, [27],
- When $r \geq d$ and the mesh is a barycentric refinement of a regular mesh, [26, 31].

This paper considers only such situations, so that (2.2) is satisfied.

A modified Stokes projection $\boldsymbol{s}_h : \boldsymbol{V} \to \boldsymbol{V}_{h,\mathrm{div}}$ is considered for the error analysis of the velocity, see [8], satisfying

$$(\nabla \boldsymbol{s}_h, \nabla \boldsymbol{v}_h) = (\nabla \boldsymbol{u}, \nabla \boldsymbol{v}_h) \quad \forall\, \boldsymbol{v}_h \in \boldsymbol{V}_{h,\mathrm{div}}. \tag{2.3}$$

The following bound holds for $m \in \{0, 1\}$, compare [8],

$$\|\boldsymbol{u} - \boldsymbol{s}_h\|_m \leq C h^{r+1-m} \|\boldsymbol{u}\|_{r+1} \quad \forall\, \boldsymbol{u} \in \boldsymbol{V} \cap \boldsymbol{H}^{r+1}(\Omega). \tag{2.4}$$

In addition, the following bounds are valid, see [13, (3.32)], [9, (21)], [6],

$$\|\boldsymbol{s}_h\|_{L^\infty} \leq C \left(\|\boldsymbol{u}\|_{d-2} \|\boldsymbol{u}\|_2\right)^{1/2}, \quad \|\nabla \boldsymbol{s}_h\|_{L^\infty} \leq C \|\nabla \boldsymbol{u}\|_{L^\infty}. \tag{2.5}$$

If $\partial_t \boldsymbol{u}$ is sufficiently regular, a modified Stokes projection of the form (2.3) can be defined for $\partial_t \boldsymbol{u}$ and error bounds of the form (2.4) can be derived for $\partial_t (\boldsymbol{u} - \boldsymbol{s}_h)$.

Let $(\boldsymbol{V}_h, Q_h)$ be a pair of Scott–Vogelius finite element spaces satisfying (2.2), then the semi-discrete problem reads as follows: Find $\boldsymbol{u}_h : (0, T] \to \boldsymbol{V}_h$ and $p_h : (0, T) \to Q_h$ such that for all $(\boldsymbol{v}_h, q_h) \in (\boldsymbol{V}_h, Q_h)$ it holds

$$\begin{aligned} \rho\,(\partial_t \boldsymbol{u}_h, \boldsymbol{v}_h) \;&+\mu\,(\nabla \boldsymbol{u}_h, \nabla \boldsymbol{v}_h) + \rho\,((\boldsymbol{u}_h \cdot \nabla)\boldsymbol{u}_h, \boldsymbol{v}_h) + \rho\,(2\boldsymbol{\omega} \times \boldsymbol{u}_h, \boldsymbol{v}_h) \\ &- (\nabla \cdot \boldsymbol{v}_h, p_h) = \langle \boldsymbol{f}, \boldsymbol{v}_h \rangle_{\boldsymbol{H}^{-1}, \boldsymbol{H}^1_0} - \rho\,(\boldsymbol{\omega} \times (\boldsymbol{\omega} \times \boldsymbol{r})\,, \boldsymbol{v}_h)\,, \\ &(\nabla \cdot \boldsymbol{u}_h, q_h) = 0, \end{aligned} \tag{2.6}$$

with an initial velocity $\boldsymbol{u}_h(0, \boldsymbol{x})$, which is an appropriate approximation of $\boldsymbol{u}_0(\boldsymbol{x})$ in $\boldsymbol{V}_h$. Integrating by parts reveals that

$$((\boldsymbol{u}_h \cdot \nabla)\boldsymbol{v}_h, \boldsymbol{v}_h) = -(\nabla \cdot \boldsymbol{u}_h, \boldsymbol{v}_h \cdot \boldsymbol{v}_h) - ((\boldsymbol{u}_h \cdot \nabla)\boldsymbol{v}_h, \boldsymbol{v}_h)\,.$$

Since $\boldsymbol{u}_h \in \boldsymbol{V}_{h,\mathrm{div}} \subset \boldsymbol{V}_{\mathrm{div}}$, the first term on the right-hand side vanishes so that

$$((\boldsymbol{u}_h \cdot \nabla)\boldsymbol{v}_h, \boldsymbol{v}_h) = 0 \quad \forall\, \boldsymbol{v}_h \in \boldsymbol{V}_h. \tag{2.7}$$

In addition, since the vector $\boldsymbol{\omega} \times \boldsymbol{v}_h$ is perpendicular to $\boldsymbol{v}_h$ for almost all $\boldsymbol{x} \in \Omega$, it is

$$(2\boldsymbol{\omega} \times \boldsymbol{v}_h, \boldsymbol{v}_h) = 0 \quad \forall\, \boldsymbol{v}_h \in \boldsymbol{V}_h. \tag{2.8}$$

For the convenience of the reader, some tools that will be used in the numerical analysis will be summarized. The first one is Young's inequality: For $a, b \geq 0$ it holds that

$$ab \leq \frac{\varepsilon}{p} a^p + \frac{\varepsilon^{-q/p}}{q} b^q \tag{2.9}$$

for any $\varepsilon > 0$, $p, q \geq 1$ with $1/p + 1/q = 1$. Hölder's inequality reads as follows: Let $f \in L^p(\Omega)$ and $g \in L^q(\Omega)$ for $1/p + 1/q = 1$ with $p, q \in [1, \infty]$. Then $fg \in L^1(\Omega)$ and

$$\|fg\|_{L^1} \leq \|f\|_{L^p} \|g\|_{L^q}. \tag{2.10}$$

For $q = p = 2$, this inequality is also known as Cauchy–Schwarz inequality. A straightforward calculation, combining Hölder's and Young's inequality, shows that

$$(\boldsymbol{\omega} \times \boldsymbol{v}, \boldsymbol{w}) \leq C_{\boldsymbol{\omega}} \|\boldsymbol{\omega}\|_{L^\infty} \|\boldsymbol{v}\|_0 \|\boldsymbol{w}\|_0 \quad \forall\, \boldsymbol{v}, \boldsymbol{w} \in \boldsymbol{H}_0^1(\Omega), \tag{2.11}$$

where $C_{\boldsymbol{\omega}} = 1$ in two dimensions and $C_{\boldsymbol{\omega}} = \sqrt{2}$ in three dimensions. Let $v \in H_0^1(\Omega)$, then Poincaré's inequality states that

$$\|v\|_0 \leq C_{\mathrm{p}} \|\nabla v\|_0, \tag{2.12}$$

where $C_{\mathrm{p}} > 0$ depends only on the domain, e.g., see [11, Theorem II.5.1].

3 Numerical analysis

This section presents the analysis of method (2.6): Consistency, energy equality, stability, and a velocity error estimate.

Lemma 3.1 *(Consistency) For any velocity solution $\boldsymbol{u}$ of (2.1) satisfying $\boldsymbol{u} \in \boldsymbol{V}_h$ for all $t > 0$ and $\boldsymbol{u}_0(\boldsymbol{x}) = \boldsymbol{u}_h(0, \boldsymbol{x})$, it holds that $\boldsymbol{u}_h(t) = \boldsymbol{u}(t)$ for all $t \in [0, T]$.*

Proof By assumption both problems (2.1) and (2.6) have the same initial condition.

A velocity field is a solution of the discrete problem if and only if it satisfies the discrete initial condition and it holds for all test functions from $\boldsymbol{V}_{h,\mathrm{div}}$

$$\begin{aligned} \rho\,(\partial_t \boldsymbol{u}_h, \boldsymbol{v}_h) + \mu\,(\nabla \boldsymbol{u}_h, \nabla \boldsymbol{v}_h) + \rho\,((\boldsymbol{u}_h \cdot \nabla)\boldsymbol{u}_h, \boldsymbol{v}_h) + \rho\,(2\boldsymbol{\omega} \times \boldsymbol{u}_h, \boldsymbol{v}_h) \\ = \langle \boldsymbol{f}, \boldsymbol{v} \rangle_{\boldsymbol{H}^{-1}, \boldsymbol{H}_0^1} - \rho(\boldsymbol{\omega} \times (\boldsymbol{\omega} \times \boldsymbol{r})\,, \boldsymbol{v}_h). \end{aligned}$$

Since for the Scott–Vogelius pair of spaces $\boldsymbol{V}_{h,\mathrm{div}} \subset \boldsymbol{V}_{\mathrm{div}}$, these test functions can be used also in the continuous problem (2.1), showing that $\boldsymbol{u}$ satisfies the same equation. □

Lemma 3.2 *(Energy equality and stability) For any velocity solution $\boldsymbol{u}_h \in \boldsymbol{V}_h$ of the spatially discretized problem (2.6) hold, for all $t \in (0, T]$, the energy equality*

$$\frac{\rho}{2}\|\boldsymbol{u}_h(t)\|_0^2 + \mu \int_0^t \|\nabla \boldsymbol{u}_h(s)\|_0^2 \,\mathrm{d}s$$
$$= \frac{\rho}{2}\|\boldsymbol{u}_h(0)\|_0^2 + \int_0^t \langle \boldsymbol{f}, \boldsymbol{u}_h(s)\rangle_{\boldsymbol{H}^{-1},\boldsymbol{H}_0^1} \,\mathrm{d}s - \rho \int_0^t (\boldsymbol{\omega}(s) \times (\boldsymbol{\omega}(s) \times \boldsymbol{r}), \boldsymbol{u}_h(s)) \,\mathrm{d}s$$

and the a priori estimate (stability estimate)

$$\rho\|\boldsymbol{u}_h(t)\|_0^2 + \mu \int_0^t \|\nabla \boldsymbol{u}_h(s)\|_0^2 \,\mathrm{d}s$$
$$\leq \rho\|\boldsymbol{u}_h(0)\|_0^2 + \frac{2}{\mu}\int_0^t \|\boldsymbol{f}(s)\|_{H^{-1}}^2 \,\mathrm{d}s + 2C(\Omega)\frac{\rho^2}{\mu}\int_0^t \|\boldsymbol{\omega}(s)\|_{L^\infty}^4 \,\mathrm{d}s, \tag{3.1}$$

where $C(\Omega)$ is a constant that depends only on the domain.

Proof Testing (2.6) by $\boldsymbol{v}_h = \boldsymbol{u}_h(s) \in \boldsymbol{V}_{h,\mathrm{div}}$, with fixed $s \in (0, T]$, and using the definition of the kinematic viscosity, (2.7), and (2.8) yields

$$\frac{\rho}{2}\frac{d}{dt}\|\boldsymbol{u}_h(s)\|_0^2 + \mu\|\nabla \boldsymbol{u}_h(s)\|_0^2 = \langle \boldsymbol{f}(s), \boldsymbol{u}_h(s)\rangle_{\boldsymbol{H}^{-1},\boldsymbol{H}_0^1} - \rho(\boldsymbol{\omega}(s) \times (\boldsymbol{\omega}(s) \times \boldsymbol{r}), \boldsymbol{u}_h(s)). \tag{3.2}$$

Integrating over the time interval $(0, t) \subset (0, T]$ gives the energy equality.

Applying the boundedness of the functional $\boldsymbol{f}$, inequality (2.11), the Poincaré inequality (2.12), and Young's inequality (2.9) on the right-hand side of (3.2) leads to

$$\begin{aligned}
&\frac{\rho}{2}\frac{d}{dt}\|\boldsymbol{u}_h(s)\|_0^2 + \mu\|\nabla \boldsymbol{u}_h(s)\|_0^2 \\
&\qquad \leq \|\boldsymbol{f}(s)\|_{H^{-1}}\|\nabla \boldsymbol{u}_h(s)\|_0 + C_{\boldsymbol{\omega}}^2\rho\|\boldsymbol{\omega}(s)\|_{L^\infty}^2\|\boldsymbol{r}\|_0\|\boldsymbol{u}_h(s)\|_0 \\
&\qquad \leq \|\boldsymbol{f}(s)\|_{H^{-1}}\|\nabla \boldsymbol{u}_h(s)\|_0 + C_{\boldsymbol{\omega}}^2 C_{\mathrm{p}}\rho\|\boldsymbol{\omega}(s)\|_{L^\infty}^2\|\boldsymbol{r}\|_0\|\nabla \boldsymbol{u}_h(s)\|_0 \\
&\qquad \leq \frac{1}{\mu}\|\boldsymbol{f}(s)\|_{H^{-1}}^2 + C(\Omega)\frac{\rho^2}{\mu}\|\boldsymbol{\omega}(s)\|_{L^\infty}^4 + \frac{\mu}{2}\|\nabla \boldsymbol{u}_h(s)\|_0^2.
\end{aligned}$$

Bounding $\|\boldsymbol{r}\|_0$, one finds that the constant on the right-hand side, which contains the factor $\|\boldsymbol{r}\|_0^2$, is

$$C(\Omega) = C_{\boldsymbol{\omega}}^4 C_{\mathrm{p}}^2 |\Omega| \max_{\boldsymbol{x}\in\overline{\Omega}} \|\boldsymbol{x}\|_2^2,$$

where $|\cdot|$ denotes the volume of Ω. The stability estimate is obtained by integrating the inequality over $(0, t) \subset (0, T]$. □

The stability estimate (3.1) shows that norms of the finite element velocity solution are bounded by data of the problem: Viscosity, density, angular velocity, body force, initial velocity, and properties of the domain.

We proceed to present an error analysis for the velocity solution of (2.6).

Theorem 3.1 *(Velocity error estimate) Assume for the solution of (2.1) that*

$$\begin{aligned}\boldsymbol{u} \in L^2\left(0,T;\boldsymbol{V}_{\mathrm{div}}\right) \cap L^2\left(0,T;\boldsymbol{H}^{r+1}(\Omega)\right) \cap L^\infty\left(0,T;\boldsymbol{H}_{\mathrm{div}}(\Omega)\right)\\ \cap L^\infty\left(0,T;\boldsymbol{H}^{\max\{2,r\}}(\Omega)\right) \cap L^1\left(0,T;\boldsymbol{W}^{1,\infty}(\Omega)\right).\end{aligned}$$

Let $\boldsymbol{u}_h$ be the velocity solution of (2.6). Then, the following error estimate holds

$$\begin{aligned}&\|(\boldsymbol{u}-\boldsymbol{u}_h)(t)\|_0^2 + \nu\|\nabla(\boldsymbol{u}-\boldsymbol{u}_h)\|^2_{L^2((0,t);L^2)}\\ &\quad\le Ch^{2r}\left(\|\boldsymbol{u}(t)\|^2_{L^\infty((0,t);H^r)} + \nu\|\nabla\boldsymbol{u}\|^2_{L^2((0,t);H^r)} + \exp\left(L(T,\boldsymbol{u})\right)M(T,\boldsymbol{u},\boldsymbol{\omega})\right)\\ &\qquad+2\exp\left(L(T,\boldsymbol{u})\right)\|\boldsymbol{u}_h(0)-\boldsymbol{s}_h(0)\|_0^2,\end{aligned} \tag{3.3}$$

for all $t \in (0,T]$ with

$$L(T,\boldsymbol{u}) = 2\int_0^T \left(\|\nabla\boldsymbol{u}\|_{L^\infty}+1\right)\,\mathrm{d}s, \tag{3.4}$$

and

$$M(T,\boldsymbol{u},\boldsymbol{\omega}) = \int_0^T \left(\|\boldsymbol{u}\|_1\|\boldsymbol{u}\|_2\|\boldsymbol{u}\|^2_{r+1} + \|\partial_t\boldsymbol{u}\|_r^2 + \|\boldsymbol{\omega}\|^2_{L^\infty}\|\boldsymbol{u}\|_r^2\right)\,\mathrm{d}s. \tag{3.5}$$

The constant C in (3.3) does not blow up as μ tends to zero.

Proof The proof follows the proof of [12, Theorem 4.7]. Denote

$$\boldsymbol{\eta} = (\boldsymbol{u}-\boldsymbol{s}_h), \quad \boldsymbol{\phi}_h = (\boldsymbol{u}_h-\boldsymbol{s}_h),$$

where $\boldsymbol{s}_h$ is the Stokes projection defined in (2.3). Hence, it is $\boldsymbol{\phi}_h \in \boldsymbol{V}_{h,\mathrm{div}}$. Then, subtracting (2.6) from (2.1) and using (2.3) leads to the error equation

$$\begin{aligned}&\rho\left(\partial_t\boldsymbol{\phi}_h,\boldsymbol{v}_h\right) + \mu\left(\nabla\boldsymbol{\phi}_h,\nabla\boldsymbol{v}_h\right) + \rho\left((\boldsymbol{u}_h\cdot\nabla)\boldsymbol{u}_h,\boldsymbol{v}_h\right) - \rho\left((\boldsymbol{s}_h\cdot\nabla)\boldsymbol{s}_h,\boldsymbol{v}_h\right)\\ &\quad+\rho\left(2\boldsymbol{\omega}\times\boldsymbol{\phi}_h,\boldsymbol{v}_h\right)\\ &= \rho\left(\partial_t\boldsymbol{\eta},\boldsymbol{v}_h\right) + \rho\left((\boldsymbol{u}\cdot\nabla)\boldsymbol{u},\boldsymbol{v}_h\right) - \rho\left((\boldsymbol{s}_h\cdot\nabla)\boldsymbol{s}_h,\boldsymbol{v}_h\right) + \rho\left(2\boldsymbol{\omega}\times\boldsymbol{\eta},\boldsymbol{v}_h\right)\end{aligned}$$

for all $\boldsymbol{v}_h \in \boldsymbol{V}_{h,\mathrm{div}}$. Note that the terms on the right-hand side of the momentum balance disappear in the derivation of the error equation. Taking $\boldsymbol{v}_h = \boldsymbol{\phi}_h$ and using (2.8) yields

$$\begin{aligned}\frac{\rho}{2}\frac{d}{dt}\|\boldsymbol{\phi}_h\|_0^2+\mu\|\nabla\boldsymbol{\phi}_h\|_0^2 \leq& \rho\left|\left((\boldsymbol{u}_h\cdot\nabla)\boldsymbol{u}_h,\boldsymbol{\phi}_h\right)-\left((\boldsymbol{s}_h\cdot\nabla)\boldsymbol{s}_h,\boldsymbol{\phi}_h\right)\right|\\&+\rho\left|\left((\boldsymbol{u}\cdot\nabla)\boldsymbol{u},\boldsymbol{\phi}_h\right)-\rho\left((\boldsymbol{s}_h\cdot\nabla)\boldsymbol{s}_h,\boldsymbol{\phi}_h\right)\right|\\&+\rho\left|\left(\partial_t\boldsymbol{\eta},\boldsymbol{\phi}_h\right)\right|+\rho\left|\left(2\boldsymbol{\omega}\times\boldsymbol{\eta},\boldsymbol{\phi}_h\right)\right|. \end{aligned}\tag{3.6}$$

The first term on the right-hand side of (3.6) is bounded by adding and subtracting $(\boldsymbol{u}_h\cdot\nabla)\boldsymbol{s}_h,\boldsymbol{\phi}_h)$, applying the triangle inequality, using the skew-symmetric property (2.7) of the nonlinear term for weakly divergence-free functions, and finally Hölder's inequality (2.10)

$$\begin{aligned}\rho|\left((\boldsymbol{u}_h\cdot\nabla)\boldsymbol{u}_h,\boldsymbol{\phi}_h\right)-\left((\boldsymbol{s}_h\cdot\nabla)\boldsymbol{s}_h,\boldsymbol{\phi}_h\right)| &\leq \rho|\left((\boldsymbol{u}_h\cdot\nabla)\boldsymbol{\phi}_h,\boldsymbol{\phi}_h\right)|+\rho|\left((\boldsymbol{\phi}_h\cdot\nabla)\boldsymbol{s}_h,\boldsymbol{\phi}_h\right)|\\&=\rho|\left((\boldsymbol{\phi}_h\cdot\nabla)\boldsymbol{s}_h,\boldsymbol{\phi}_h\right)|\\&\leq\rho\|\nabla\boldsymbol{s}_h\|_{L^\infty}\|\boldsymbol{\phi}_h\|_0^2.\end{aligned}$$

For bounding the second term on the right-hand side of (3.6), $((\boldsymbol{s}_h\cdot\nabla)\boldsymbol{u},\boldsymbol{\phi}_h)$ is added and subtracted, Hölder's inequality (2.10), the Sobolev embeddings $H^1(\Omega)\to L^6(\Omega)$ and $H^{1/2}(\Omega)\to L^3(\Omega)$, see [1, Theorem 5.4], a Sobolev interpolation theorem, see [1, Theorem 4.17], (2.5), and (2.4) are used to obtain

$$\begin{aligned}&\rho\left|\left((\boldsymbol{u}\cdot\nabla)\boldsymbol{u},\boldsymbol{\phi}_h\right)-\rho\left((\boldsymbol{s}_h\cdot\nabla)\boldsymbol{s}_h,\boldsymbol{\phi}_h\right)\right|\\&\leq\rho\left|\left((\boldsymbol{\eta}\cdot\nabla)\boldsymbol{u},\boldsymbol{\phi}_h\right)\right|+\left|\left(\boldsymbol{s}_h\cdot\nabla)\boldsymbol{\eta},\boldsymbol{\phi}_h\right)\right|\\&\leq\rho\|\boldsymbol{\eta}\|_{L^6}\|\nabla\boldsymbol{u}\|_{L^3}\|\boldsymbol{\phi}_h\|_0+\|\boldsymbol{s}_h\|_{L^\infty}\|\nabla\boldsymbol{\eta}\|_0\|\boldsymbol{\phi}_h\|_0\\&\leq C\rho\left(\|\nabla\boldsymbol{u}\|_{1/2}+\|\boldsymbol{s}_h\|_{L^\infty}\right)\|\boldsymbol{\eta}\|_1\|\boldsymbol{\phi}_h\|_0\\&\leq C\rho\left((\|\boldsymbol{u}\|_1\|\boldsymbol{u}\|_2)^{1/2}+\|\boldsymbol{s}_h\|_{L^\infty}\right)\|\boldsymbol{\eta}\|_1\|\boldsymbol{\phi}_h\|_0\\&\leq C\rho h^r(\|\boldsymbol{u}\|_1\|\boldsymbol{u}\|_2)^{1/2}\|\boldsymbol{u}\|_{r+1}\|\boldsymbol{\phi}_h\|_0.\end{aligned}$$

The third term on the right-hand side of (3.6) is estimated by applying the Cauchy–Schwarz inequality (2.10) and (2.4) for the temporal derivative

$$\rho\left|\left(\partial_t\boldsymbol{\eta},\boldsymbol{\phi}_h\right)\right|\leq\rho\|\partial_t\boldsymbol{\eta}\|_0\|\boldsymbol{\phi}_h\|_0\leq C\rho h^r\|\partial_t\boldsymbol{u}\|_r\|\boldsymbol{\phi}_h\|_0.$$

And the last term is estimated similarly, using (2.11),

$$\rho\left|\left(2\boldsymbol{\omega}\times\boldsymbol{\eta},\boldsymbol{\phi}_h\right)\right|\leq 2\rho C_\omega\|\boldsymbol{\omega}\|_{L^\infty}\|\boldsymbol{\eta}\|_0\|\boldsymbol{\phi}_h\|_0\leq C\rho h^r\|\boldsymbol{\omega}\|_{L^\infty}\|\boldsymbol{u}\|_r\|\boldsymbol{\phi}_h\|_0.$$

Inserting all estimates, applying Young's inequality (2.9) to all bounds where $\|\boldsymbol{\phi}_h\|_0$ appears only linearly, and multiplying with $2/\rho$ gives

$$\begin{aligned}\frac{d}{dt}\|\boldsymbol{\phi}_h\|_0^2+2\nu\|\nabla\boldsymbol{\phi}_h\|_0^2\leq Ch^{2r}\left(\|\boldsymbol{u}\|_1\|\boldsymbol{u}\|_2\|\boldsymbol{u}\|_{r+1}^2+\|\partial_t\boldsymbol{u}\|_r^2+\|\boldsymbol{\omega}\|_{L^\infty}^2\|\boldsymbol{u}\|_r^2\right)\\+2(\|\nabla\boldsymbol{s}_h\|_{L^\infty}+1)\|\boldsymbol{\phi}_h\|_0^2.\end{aligned}$$

By the regularity assumptions, all terms in the parentheses are in $L^1(0, T)$, so that Gronwall's lemma, e.g., see [20, Lemma A55], can be applied. One obtains for any $t \in (0, T]$

$$\begin{aligned}&\|\boldsymbol{\phi}_h(t)\|_0^2 + 2\nu\|\nabla\boldsymbol{\phi}_h\|^2_{L^2((0,t);L^2)}\\ &\leq \exp\left(L(T,\boldsymbol{u})\right)\|\boldsymbol{\phi}_h(0)\|_0^2 + Ch^{2r}\exp\left(L(T,\boldsymbol{u})\right)M(T,\boldsymbol{u},\boldsymbol{\omega}),\end{aligned}$$

where $L(T, \boldsymbol{u})$ and $M(T, \boldsymbol{u}, \boldsymbol{\omega})$ are defined in (3.4) and (3.5), respectively.

The application of the triangle inequality concludes the proof. □

In contrast to the robustness of the error (3.3) with respect to small viscosity coefficients, the bound blows up if the angular velocity increases. It can be seen that the predicted blow-up is not exponential but linear for one term of the error bound [note that the square of the error is considered in (3.3)].

4 Numerical studies

This section presents numerical studies to illustrate the behavior of method (2.6) and to verify the theoretical results.

4.1 Problem with prescribed solution

Convergence rates are usually supported with examples that have a prescribed solution, e.g., see [25] for the Navier–Stokes equations with Coriolis force. To this end, we considered (1.1) with the prescribed velocity solution $\boldsymbol{u} = (u_1, u_2)^T$ with

$$\begin{aligned}u_1 &= \pi\sin(t)\sin(2\pi y)\sin^2(\pi x),\\ u_2 &= -\pi\sin(t)\sin(2\pi x)\sin^2(\pi y).\end{aligned} \tag{4.1}$$

Simulations were performed in the unit square $\Omega = (0, 1)^2$ and with the final time $T = 1$. The angular velocity was chosen to be a constant vector in our simulations. Then, the centripetal force can be written as a gradient, see (1.2), so that this force can be incorporated in the pressure. We performed this approach for this example, such that we obtained a modified pressure $p - \phi_c$. An approximation of the actual pressure can be computed in a post-processing step using (1.2). The modified pressure was chosen to be

$$p - \phi_c = \sin(t)\cos(\pi x)\sin(\pi y). \tag{4.2}$$

Then the external force $\boldsymbol{f}$, the Dirichlet boundary condition, and the initial condition were determined by (4.1) and (4.2). We considered $\rho = 1\,\mathrm{kg/m^3}$ and simulations with different values of μ and $\boldsymbol{\omega}$ were performed. Note that in two dimensions the angular velocity is $\boldsymbol{\omega} = \omega\boldsymbol{e}_z$, where $\boldsymbol{e}_z$ is the Cartesian unit vector in z-direction.

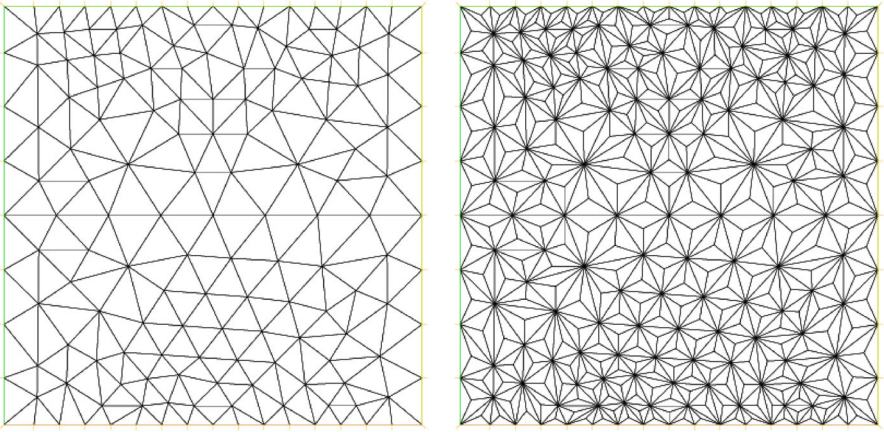

Fig. 1 Problem with prescribed solution. Example of an unstructured grid (left) and the corresponding barycentric-refined grid (right)

Table 1 Problem with prescribed solution

Level	#triangles	#dof $\boldsymbol{u}_h$	#dof p_h
1	276	1154	828
2	810	3338	2430
3	3192	12962	9576
4	12822	51674	38466

Number of mesh cells and number of degrees of freedom for (P_2, P_1^{disc})

As spatial discretization, the Scott–Vogelius pair (P_2, P_1^{disc}), i.e., $r = 2$, defined on barycentric-refined grids was used. Let a positive number N be given and define the size of the equidistant time step by $\Delta t = T/N$. In order that the temporal discretization error is negligible, the very small time step $\Delta t = 0.0001$ was applied, hence the number of time steps is $N = 10000$. Quantities at time step $t^n = n\Delta t$ are denoted with a superscript n. As temporal discretization, the second order linearly extrapolated backward differentiation formula (BDF2LE), i.e., replacing the first factor in the convective term $\boldsymbol{u}_h^{n+1} \cdot \nabla \boldsymbol{u}_h^{n+1}$ with the extrapolation $(2\boldsymbol{u}_h^n - \boldsymbol{u}_h^{n-1})$, was used. The initial velocity was $\boldsymbol{u}_h(0) = \boldsymbol{0}$. In the first time step, a dummy velocity $\boldsymbol{u}_h(-\Delta t)$, being the Lagrangian interpolant of (4.1) for $t = -\Delta t$, was used as a second initial value.

We computed numerical solutions on successively refined unstructured meshes. An example of such a mesh and the corresponding barycentric-refined mesh can be seen in Fig. 1. Information concerning the number of degrees of freedom are provided in Table 1.

The simulations were performed with the finite element software package FreeFem++ [15], where the UMFPACK sparse direct linear solver [7] was applied for solving the linear systems of equations.

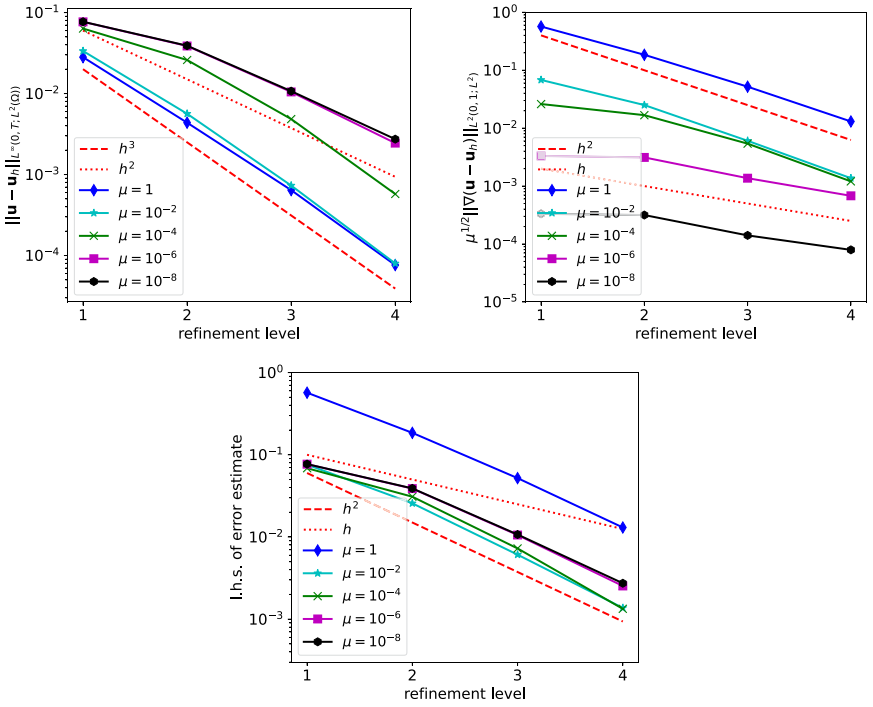

Fig. 2 Problem with prescribed solution. Velocity errors for varying viscosity μ and fixed $\omega = 1$ with the Scott–Vogelius pair (P_2, P_1^{disc}). The bottom picture is for the square root of the left-hand side of error estimate (3.3)

The studied errors are given by

$$\|\boldsymbol{u} - \boldsymbol{u}_h\|_{\ell^\infty(L^2)} = \max_{t^n \in [0,T]} \|(\mathbf{u} - \mathbf{u}_h)(t^n)\|_{L^2}, \tag{4.3}$$

$$\mu^{1/2} \|\nabla(\mathbf{u} - \mathbf{u}_h)\|_{L^2([0,1];L^2)} = \left(\mu \sum_{n=1}^{N} \Delta t \|\nabla(\mathbf{u}(t^n) - \mathbf{u}_h^n)\|_{L^2}^2 \right)^{1/2}, \tag{4.4}$$

and the square root of the term on the left-hand side of (3.3) (which is abbreviated with 'l.h.s. of error estimate').

We first performed a study for varying viscosity $\mu \in \{1, 10^{-2}, 10^{-4}, 10^{-6}, 10^{-8}\}$ with fixed angular velocity $\omega = 1$, see Fig. 2. This study aimed to check the robustness of the errors with respect to small viscosity coefficients. This kind of robustness of the error on the left-hand side of (3.3) as well as the predicted second order of convergence of this term can be clearly observed. With respect to the error in $\ell^\infty(L^2)$ defined in (4.3), a small increase can be observed if the viscosity decreases, but not a blow-up. Apart of the two smallest viscosity coefficient, third order convergence can be already seen. The error given in (4.4) is robust. For all but the two smallest viscosity coefficients, the second order convergence is already visible.

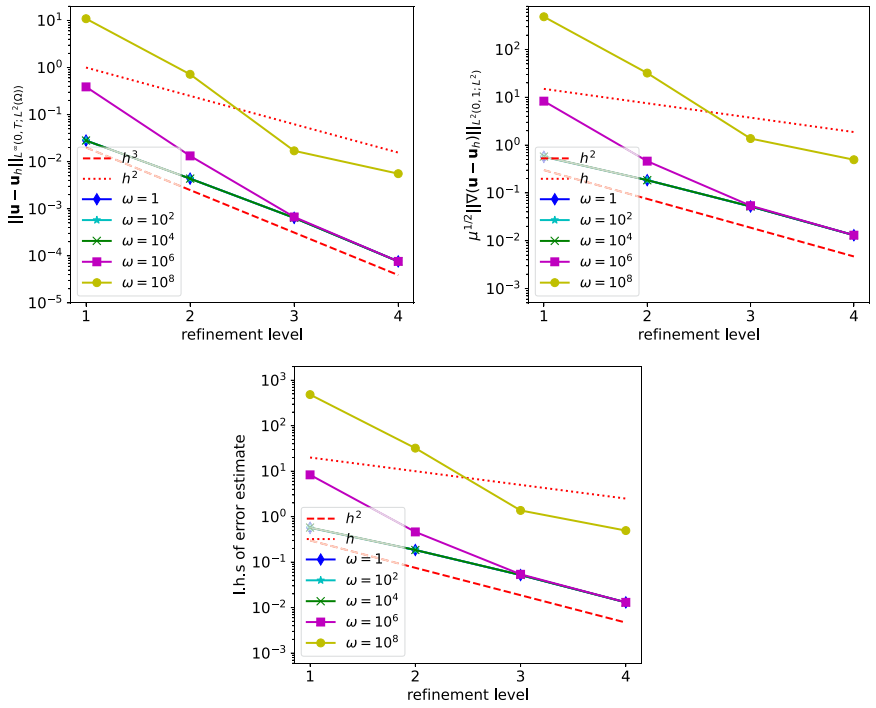

Fig. 3 Problem with prescribed solution. Velocity errors for fixed $\mu = 1$ and varying ω with the Scott–Vogelius pair (P_2, P_1^{disc}). The bottom picture is for the square root of the left-hand side of error estimate (3.3)

The second study was for fixed $\mu = 1$ and varying $\omega \in \{1, 10^2, 10^4, 10^6, 10^8\}$. In this case the error bound (3.3) predicts a linear dependency on the angular velocity. This effect can be seen in Fig. 2 for the largest angular velocity $\omega = 10^8$, where all errors are around two orders of magnitude larger than for $\omega = 10^6$. Apart of the largest angular velocity, one can observe for all errors the optimal order of convergence already on the considered coarse grids, in particular for the error on the left-hand side of estimate (3.3).

In summary, both the pressure robustness and the linear dependency on ω (at least for large angular velocities) can be observed in the numerical results.

4.2 Rotating cylinder problem

This problem is inspired from [4], where simulations for $\boldsymbol{\omega} = \omega \boldsymbol{e}_z$ with $\omega \leq 1$ are presented, which were performed with the Taylor–Hood (P_2, P_1) pair of finite element spaces. The computational flow domain is an annular area, with center $(0, 0)$, between an inner circle with radius 0.75 m and an outer circle with radius 1 m. The inner radius is taken with the rotational speed ω and the outer radius is stationary. Rotation is considered positive in the counterclockwise direction. In the rotating frame of reference, the inner cylinder has no-slip boundary conditions $\boldsymbol{u} = \boldsymbol{0}$.

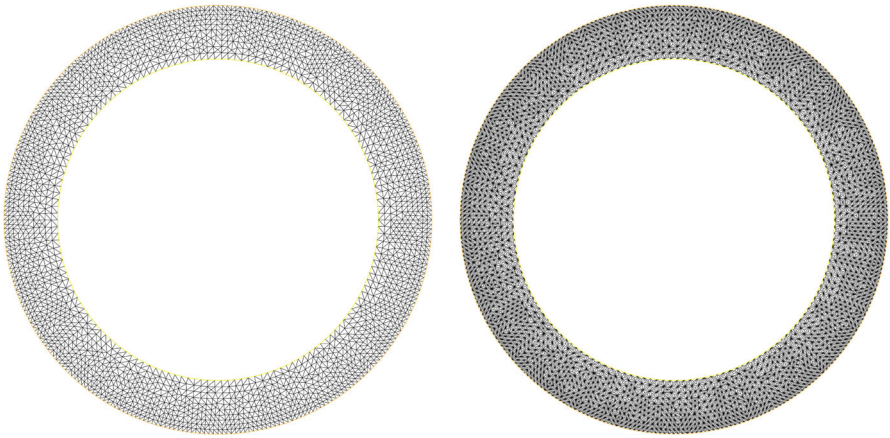

Fig. 4 Rotating cylinder problem. The unstructured triangular mesh (left) and its barycentric refinement (right)

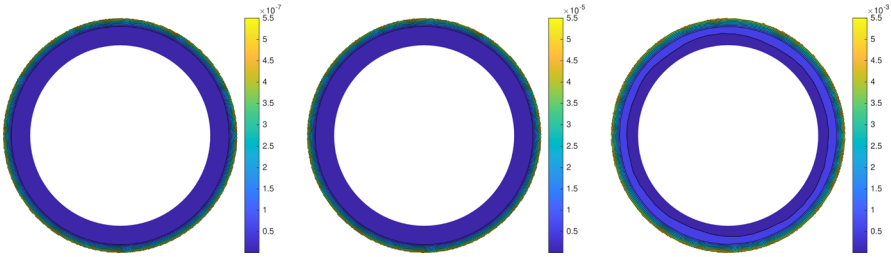

Fig. 5 Rotating cylinder problem. Velocity magnitude distribution at $t = 10$ for $\omega \in \{1, 10, 10^2\}\varphi(t)$ (left to right) with the Scott–Vogelius pair (P_2, P_1^{disc})

We consider this setup as a numerical approach for an exterior domain problem, where this problem is defined in $\mathbb{R}^2 \backslash \{\boldsymbol{x} \ : \ \|\boldsymbol{x}\|_2 \leq 0.75\}$. Then the outer circle is just an artificial boundary, introduced for being able to apply standard finite element spaces. On this boundary, we prescribed the standard do-nothing boundary condition.

For the simulations, the term with the centripetal force was considered on the right-hand side of the equation, i.e., it was not incorporated into the pressure term. Since the angular velocity is constant, the centripetal force can be rewritten as a gradient, see (1.2). Then, the expectation for a solution is that this gradient is balanced by the pressure gradient and that the velocity field in the rotating frame of reference is zero, at least away from the artificial boundary. In a neighborhood of the outer circle there might be an impact on the numerical solution from the artificial boundary.

We ran the problem on an unstructured mesh, see Fig. 4, leading to 58020 velocity degrees of freedom and 42840 pressure degrees of freedom with an end time $T = 10$. Like in [4], the density $\rho = 1$ kg/m^3 and the dynamic viscosity $\mu = 10^{-2}$ kg/ms were used. Simulations were performed for $\omega \in \{1, 10, 10^2\}\varphi(t)$ with $\varphi(t) = t$ for $t \in [0, 1]$ and $\varphi(t) = 1$ else. The BDF2LE scheme was applied with the time step $\Delta t = 10^{-2}$ and with the zero initial conditions in $t \in \{-\Delta t, 0\}$.

Results are presented in Figs. 5 and 6. It can be seen that the expectations are met. In particular, the velocity field is close to zero away from the artificial boundary. The

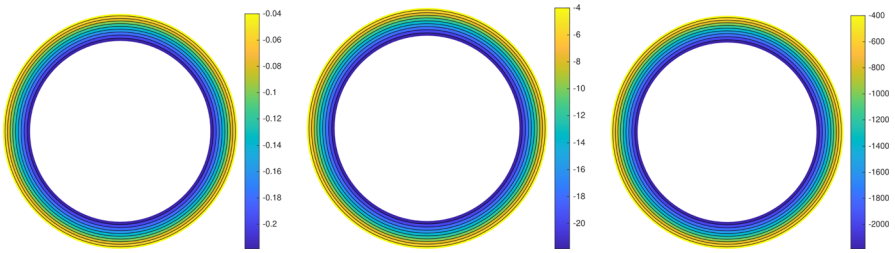

Fig. 6 Rotating cylinder problem. Pressure distribution at $t = 10$ for $\omega \in \{1, 10, 10^2\}\varphi(t)$ (left to right) with the Scott–Vogelius pair (P_2, P_1^{disc})

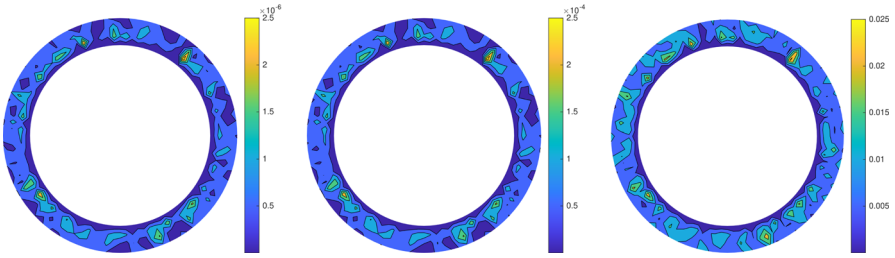

Fig. 7 Rotating cylinder problem. Velocity magnitude distribution at $t = 10$ for $\omega \in \{1, 10, 10^2\}\varphi(t)$ (left to right) with the Taylor–Hood pair (P_2, P_1)

Table 2 Rotating cylinder problem as no-flow problem

μ	$\|\boldsymbol{u} - \boldsymbol{u}_h\|_{\ell^\infty(L^2)}$	$\mu^{1/2}\|\nabla(\mathbf{u} - \mathbf{u}_h)\|_{L^2([0,1];L^2)}$	(l.h.s. of (3.3))$^{1/2}$
1	$5.87672 \cdot 10^{-11}$	$2.26296 \cdot 10^{-9}$	$2.26372 \cdot 10^{-9}$
10^{-2}	$7.35792 \cdot 10^{-10}$	$2.66913 \cdot 10^{-9}$	$2.76869 \cdot 10^{-9}$
10^{-4}	$1.00156 \cdot 10^{-8}$	$2.26577 \cdot 10^{-9}$	$1.02687 \cdot 10^{-8}$
10^{-6}	$1.07673 \cdot 10^{-8}$	$2.40232 \cdot 10^{-10}$	$1.07699 \cdot 10^{-8}$
10^{-8}	$1.07752 \cdot 10^{-8}$	$2.40394 \cdot 10^{-11}$	$1.07752 \cdot 10^{-8}$

Velocity errors for fixed $\omega = 10$ and varying μ with the Scott–Vogelius pair (P_2, P_1^{disc})

impact of this boundary is the greater the larger ω is. If the value of ω becomes too large, we have observed a blow-up of simulations. The artificial boundary is too close to the inner circle for such situations and for approximating the solution of an exterior domain problem, one would need to use a larger radius for the outer circle. In addition, the pressure becomes the larger the larger the angular velocity is and it behaves like $\mathcal{O}(\omega^2)$ as the centripetal force.

As comparison, velocity fields obtained with the Taylor–Hood pair of spaces (P_2, P_1) are presented in Fig. 7. The simulations were performed on a grid that leads to 89780 velocity degrees of freedom and to 11465 pressure degrees of freedom, so that the total number of degrees of freedom is comparable to that for the simulations with the Scott–Vogelius pair. It can be well observed in Fig. 7 that the computed velocity fields have spurious modes, which are not present in the fields obtained with the Scott–Vogelius pair of spaces.

Finally, to quantify the pressure robustness of the Scott–Vogelius pair of finite element spaces, we considered this example with homogeneous Dirichlet boundary conditions at both the inner and outer radius, so that

$$\boldsymbol{u} = \boldsymbol{0}, \quad p = \frac{\rho\omega^2}{2}\boldsymbol{r}^2 - \frac{175}{1024}\rho\omega^2\pi$$

is the solution of the problem. For the numerical simulations, the same setup as described above was used. The velocity errors for this no-flow problem are presented in Table 2 and they clearly show that these errors are very small for all values of the viscosity coefficient.

5 Conclusion

This paper studied a finite element discretization of the Navier–Stokes equations in a rotating frame of reference. To this end, the classical Scott–Vogelius pairs of finite element spaces were considered, which lead to weakly divergence-free velocity solutions. As main result, it was shown that the velocity error in a standard norm can be bounded with the expected order of convergence and in a pressure-robust way. The error bound is also convection-robust in the sense that it does not explicitly contain inverse powers of the viscosity. One term of the error bound depends linearly on the angular velocity. The theoretical results were validated with numerical studies.

Funding Open Access funding enabled and organized by Projekt DEAL.

References

1. Adams, R.A.: Sobolev spaces. Academic Press [A subsidiary of Harcourt Brace Jovanovich, Publishers], New York-London. Pure Appl. Math. **65** (1975)
2. Akbaş, M.: On the long-time stability of finite element solutions of the Navier–Stokes equations in a rotating frame of reference. Bitlis Eren Üniversitesi Fen Bilimleri Dergisi **9**(2), 549–560 (2020)
3. Ballal, B.Y., Rivlin, R.S.: Flow of a Newtonian fluid between eccentric rotating cylinders: inertial effects. Arch. Ration. Mech. Anal. **62**(3), 237–294 (1976)
4. Boz, A.M.: Simulating the Navier–Stokes equations in the rotating frame of reference using finite element method. Master's thesis, Politecnico di Milano, Scuola di Ingegneria Industriale e dell'Informazione (2021)
5. Case, M.A., Ervin, V.J., Linke, A., Rebholz, L.G.: A connection between Scott–Vogelius and grad-div stabilized Taylor–Hood FE approximations of the Navier–Stokes equations. SIAM J. Numer. Anal. **49**(4), 1461–1481 (2011)

6. Chen, H.: Pointwise error estimates for finite element solutions of the Stokes problem. SIAM J. Numer. Anal. **44**(1), 1–28 (2006)
7. Davis, T.A.: Algorithm 832: UMFPACK V4.3–an unsymmetric-pattern multifrontal method. ACM Trans. Math. Softw. **30**(2), 196–199 (2004)
8. de Frutos, J., García-Archilla, B., John, V., Novo, J.: Grad-div stabilization for the evolutionary Oseen problem with inf-sup stable finite elements. J. Sci. Comput. **66**(3), 991–1024 (2016)
9. de Frutos, J., García-Archilla, B., John, V., Novo, J.: Analysis of the grad-div stabilization for the time-dependent Navier–Stokes equations with inf-sup stable finite elements. Adv. Comput. Math. **44**(1), 195–225 (2018)
10. Feng, Schunxin, Li, Qibing, Song, Fu.: On the orbital motion of a rotating inner cylinder in annular flow. Int. J. Numer. Methods Fluids **54**, 155–173 (2007)
11. Galdi, G.P.: An introduction to the mathematical theory of the Navier–Stokes equations. Springer Monographs in Mathematics. Springer, New York, second edition. Steady-state problems (2011)
12. García-Archilla, B., John, V., Novo, J.: On the convergence order of the finite element error in the kinetic energy for high Reynolds number incompressible flows. Comput. Methods Appl. Mech. Eng. **385**, 114032 (2021)
13. García-Archilla, B., Novo, J., Titi, E.S.: Uniform in time error estimates for a finite element method applied to a downscaling data assimilation algorithm for the Navier-Stokes equations. SIAM J. Numer. Anal. **58**(1), 410–429 (2020)
14. Giga, Y., Inui, K., Mahalov, A., Saal, J.: Uniform global solvability of the rotating Navier–Stokes equations for nondecaying initial data. Indiana Univ. Math. J. **57**(6), 2775–2791 (2008)
15. Hecht, F.: New development in freefem++. J. Numer. Math. **20**(3–4), 251–265 (2012)
16. Hieber, M., Shibata, Y.: The Fujita-Kato approach to the Navier–Stokes equations in the rotational framework. Math. Z. **265**(2), 481–491 (2010)
17. Hirt, C.W., Amsden, A.A., Cook, J.L.: An arbitrary Lagrangian–Eulerian computing method for all flow speeds. J. Comput. Phys. **14**(3), 227–253 (1974)
18. Hirt, C.W., Amsden, A.A., Cook, J.L.: An arbitrary Lagrangian–Eulerian computing method for all flow speeds. J. Comput. Phys. **135**(2), 198–216 (1997). (**With an introduction by L. G. Margolin, Commemoration of the 30th anniversary**)
19. Iwabuchi, T., Takada, R.: Global well-posedness and ill-posedness for the Navier–Stokes equations with the Coriolis force in function spaces of Besov type. J. Funct. Anal. **267**(5), 1321–1337 (2014)
20. John, V.: Finite Element Methods for Incompressible Flow Problems. Springer Series in Computational Mathematics, vol. 51. Springer, Cham (2016)
21. John, V., Linke, A., Merdon, C., Neilan, M., Rebholz, L.G.: On the divergence constraint in mixed finite element methods for incompressible flows. SIAM Rev. **59**(3), 492–544 (2017)
22. Konieczny, P., Yoneda, T.: On dispersive effect of the Coriolis force for the stationary Navier–Stokes equations. J. Differ. Equ. **250**(10), 3859–3873 (2011)
23. Linke, A., Matthies, G., Tobiska, L.: Robust arbitrary order mixed finite element methods for the incompressible Stokes equations with pressure independent velocity errors. ESAIM Math. Model. Numer. Anal. **50**(1), 289–309 (2016)
24. Olshanskii, M.A., Reusken, A.: Grad-div stabilization for Stokes equations. Math. Comput. **73**(248), 1699–1718 (2004)
25. Olshanskii, M.A., Sokolov, A., Turek, S.: Error analysis of a projection method for the Navier–Stokes equations with Coriolis force. J. Math. Fluid Mech. **12**(4), 485–502 (2010)
26. Qin, J.: On the Convergence of Some Low Order Mixed Finite Elements for Incompressible Fluids. PhD thesis, Department of Mathematics, Pennsylvania State University (1994)
27. Scott, L.R., Vogelius, M.: Conforming finite element methods for incompressible and nearly incompressible continua. In: Large-scale computations in fluid mechanics, Part 2 (La Jolla, Calif., 1983), volume 22 of Lectures in Appl. Math., pp. 221–244. Am. Math. Soc., Providence, RI (1985)
28. Shuai, C., Teng, K., Jia, H.: On the error estimates of a new operator splitting scheme for the Navier–Stokes equations with Coriolis force. Math. Probl. Eng. **2012**, 105735 (2012)
29. Sokolov, A.: Analysis and numerical realisation of discrete projection methods for rotating incompressible flows. PhD thesis, TU Dortmund, Germany (2008)
30. Sun, H.Y., Song, L.Y., Jia, H.E.: Error analysis of the incremental pressure-correction projection scheme for the Navier–Stokes equations with Coriolis force. Gongcheng Shuxue Xuebao **28**(4), 482–488 (2011)
31. Zhang, S.: A new family of stable mixed finite elements for the 3D Stokes equations. Math. Comput. **74**(250), 543–554 (2005)